

3D Coupled Stress-Flow Analysis of Jointed Rock Mass Beneath a Concrete Dam

*Moataz A. Al-Obaydi*¹, *N. K. Samadhiya*² and *M. N. Viladkar*²

1. Dept. of Civil Engineering, College of Engineering,
University of Mosul, Mosul, Iraq

2. Dept. of Civil Engineering, Indian Institute of Technology
Roorkee, Roorkee, India

Abstract

The steady state flow through the foundation jointed rock mass of a dam in identify as the key factor of stability. A hydromechanical formulation based on the continuum approach has been proposed. Darcy's law has been applied using the cubic law to simulate the flow through the joints. A software package based on finite element method has been developed to solve three-dimensional coupled stress-flow problems of anisotropic media founded beneath hydraulic structures. A test problem considered a concrete dam rested on the rock mass intersects by two joint sets. It has been found that the pattern of equipotential lines changes as a result of stress redistribution upon the loading from dam construction. The steepest joint set showed a prevailing affect on the flow pattern. Variation in pore water pressure is directly proportional to the changes in the joint aperture. The displacements slightly increase upon the flow of the water. Pattern of both the displacement and stresses remain almost unchanged when water seep in the jointed media. Through examining the effect of mechanical properties of jointed rock mass found that the stiffnesses value of the joint has a pronounced effect on the hydraulic behavior. Finally, the results show the capability of the proposed software to analyze the stress-flow interaction under the dams. A good agreement has been achieved with the results obtained by other from BRIG3D model.

Keywords: Hydraulic structures; Dams; Unconfined flow; Finite element analysis; Rock mass

Introduction

Various structures have been constructed in/on the fractured media and therefore various research workers paid more attention to the interaction between the fractures and that of structures experiencing the flow of water. The behavior was recorded in terms of displacements, stresses, stability and the

working of the structures. Several case studies have been undertaken by various research workers to check the stability of various hydraulic structures under flow of water condition. On the basis of their study of the influence of seepage and uplift forces on the stresses and displacements in the rock foundation of concrete dam, Wittke et al. (1985) found that shear stresses resulting from seepage flow are more extensive than those resulting from water pressure.

Based on experimental data, Gale (1990) found a change in fracture of the order of 3rd power of the aperture at low normal stress, indicating that the hydraulic aperture changes more rapidly than the measured fracture closure.

In 1992, the Electrical Power Research Institute in the United States completed a study of 17 existing concrete gravity dams resting on different rock foundation geology (REMR, 1996). The aim of this study was to identify key factors influencing the uplift pressures. Measurement of the uplift pressures below each of these dams showed that the foundation geology has a strong influence on the uplift pressure distribution and that the geology controls the response of the uplift pressure to the changes in dam loading. The shape and size of rock joints have also influenced the uplift pressure distribution. The effect of joint water pressure on the factor of safety against sliding was examined by Hatzor and Goodman (1997) who demonstrated that with increase in joint water pressure, the orientation of the resultant dictates a changing mode from double plane to a single plane sliding and reduces the factor of safety.

The coupled stress-permeability relationship for anisotropic fractured porous rocks was proposed by Chen and Bai (1998). The strong stress-dependency of permeability changes in a three dimensional fractured network was observed where fracture can be arbitrarily oriented. Fluid flow within a planar fracture was simulated using an analogy of flow between two parallel plates.

A three-dimensional coupled mechanical-hydraulic model for jointed rock mass of dam foundation was presented by Bargui et al. (1998). A computational model called BRG3D consisted of a three-dimensional static distinct element model as well as a hydraulic model. A cubic law was used to relate hydraulic conductivity of any interface to its hydraulic aperture. Instability condition may be induced in the foundation of dam due to changes in hydraulic behavior, especially in high compression area.

From experimental findings, Jing and Hudson (2004) indicated that the joint roughness was a decisive factor in all aspects of hydromechanical behavior of rock fractures. The conventional parallel shear-flow tests were found to be not adequate for representing the general stress-flow behavior of rock fractures. On the other hand, numerical analysis showed that hydromechanical properties of the rock fractures are stress-path dependent. This is due to the effect of anisotropic roughness on aperture evolution.

In the present study, the coupled stress-flow of jointed rock mass founded beneath the dam has been carried out. The study based on the continuum approach using 3D-finite element code incorporated in software package developed in the present study. An example has been solved to be verified the method proposed herein.

Constitutive Modelling

The aperture is a function of stresses on joint plane, hence, the permeability is stress dependent. Based on that, closure/opening of the joints may be calculated due to the changes in the loading of the media.

Depending on the type of normal stress acting on the joint plane (tensile or compressive), σ_n , the joint either exhibited a closure or opening. This behavior may be expressed by the following formula:

$$u_n = \frac{\sigma_n}{k_n} \quad (1)$$

where, u_n is the amount of joint closure may be positive (joint opening) or negative (joint closure) depending upon the normal stress being either tensile or compressive, and σ_n is the normal stress on the joint plane, and k_n is the normal stiffness of the rock joints.

In case of rough joint surfaces, the joint exhibited a dilatancy behavior as,

$$u_d = u_s \tan \beta \quad (2)$$

where, u_d is the amount of dilatancy of joint, u_s is the shear displacement along the plane of the joint, and β is the dilatancy angle. The shear displacement, u_s is calculated according to the following relation:

$$u_s = \frac{\tau}{k_s} \quad (3)$$

where, τ indicates the shear stresses in directions parallel to the joint plane at the interfaces, and k_s refers to the shear stiffness of the joints.

Hence, the aperture has been updated at each step of loading as,

$$e_i = e_0 \pm u_n + u_d \quad (4)$$

where, e_i is the adjusted value of joint aperture, and e_0 is the initial value of aperture.

Subsequently, the hydraulic conductivity of the rock joints has been updated using the following equation:

$$\kappa = \frac{\gamma_w e_i^3}{12 \mu S R_c} \quad (5)$$

where, κ is the updated value of hydraulic conductivity, γ_w is the unit weight of water, μ is the dynamic viscosity of fluid (water in this study), S is the distance (spacing) between joints in one joint set, and R_c refers to the roughness coefficient factor.

The element hydraulic conductivity matrix $[H^e]$ evaluated as,

$$[H^e] = \begin{bmatrix} \kappa_p & 0 & 0 \\ 0 & \kappa_p & 0 \\ 0 & 0 & \kappa_n \end{bmatrix} \quad (6)$$

where, κ_p is the hydraulic conductivity along the joint plane, and κ_n is the hydraulic conductivity normal to the joint plane.

Then, the hydraulic head at each nodal points can be evaluated using the following equation:

$$[H] \{\Phi\} = \{Q\} \quad (7)$$

where, $[H]$ is the global hydraulic conductivity matrix included the both hydraulic conductivity of rock material and rock joints, $\{\Phi\}$ is the nodal head vector, and $\{Q\}$ is the discharge vector. After which the pore water pressure is obtained.

In-situ and induced effective stresses have been evaluated using conventional soil mechanics formula as,

$$\sigma' = \sigma - P_w \quad (8)$$

where, σ' is the effective stress, σ represents the total stress, and P_w is the pore water pressure.

The mechanical properties of the jointed rock masses are modified with the changing in stresses. The stress dependent modulus of deformation for rock material has been taken into account using the extension of 2D formula suggested by Janbu (1963) 3D by including the intermediate stresses, σ_2 , in the relation as follows:

$$E_r = E_i \left[\frac{\sigma_2 + \sigma_3}{2 P_a} \right]^n \quad (9)$$

where, E_r is the pressure dependent modulus of rock material in triaxial condition, E_i is the modulus of deformation corresponding to unit confining pressure, σ_2 and σ_3 are the intermediate and minor principal stresses, P_a represents the atmospheric pressure, and n refers to the modulus exponent obtained from triaxial tests conducted at different confining pressures (approximately 0.15 for hard rocks, 0.30 for medium rocks and 0.50 for very soft rocks).

In addition, two models considered the shear stiffness to be the function of stresses at the interfaces of the rock joints have been considered in the proposed code (Bandis et al., 1983 and Oda et al., 1993). These models are:

$$k_n = k_{ni} \left[1 - \frac{\sigma_n}{\delta_m k_{ni} + \sigma_n} \right]^{-2} \quad (10)$$

$$\text{and } k_s = k_n / 10 \quad (11)$$

where, k_n is the normal stiffness at any stress level, k_{ni} is the initial normal stiffness, i.e. at zero stress level, σ_n is the normal stress, δ_m is maximum possible joint closure, and k_s refers to shear stiffness at any stress level.

Accordingly, the element stiffness matrix, which is a function of modulus of elasticity of rock material and the stiffnesses of rock joints, has been revised with the respect to the stress variation in coupled stress-flow analysis.

Simulation Process

The solution algorithm which is adopted in the coupled stress-flow analysis, can be explained using the following steps:

- i. The stress analysis is carried out in the media treating rock mass as in dry condition. Both stresses and deformations in terms of total stresses, σ , i.e. zero pore water pressure, P_w , are evaluated for the domain under consideration.

ii. All calculations like compliance matrices, element stiffness matrices and the traction forces on the excavated surface are based on the total stresses.

iii. For first iteration ($i = 1$), adjust the amount of the joint aperture, \bar{e} according to:

$$\bar{e}_i = f(\sigma) \quad (12)$$

iv. Then, the hydraulic characteristics are evaluated in the seepage analysis based on the stresses and deformations derived from stress analysis. In this step, the total hydraulic head, Φ at each nodal point is obtained (eq. 7).

v. The piezometric head, ϕ_w at any nodal point in the finite element mesh may be evaluated by subtracting the elevation head, h_z of any nodal point from the total hydraulic head, Φ of that nodal point.

$$\{\phi_w^i\} = \{\Phi^i\} - \{h_z^i\} \quad (13)$$

Pore water pressure, P_w at each nodal point is evaluated according to the following formulae:

$$\{P_w^i\} = \gamma_w \{\phi_w^i\} \quad (14)$$

vi. Thereafter, the pore water pressures calculated in step (v) are subtracted from the total stresses to obtain the effective in-situ (initial) stresses as,

$$\{\sigma'_{i+1}\} = \{\sigma_i\} - \{P_w^i\} \quad (15)$$

vii. Adjust the values of parameters which are stress-dependent such as modulus of elasticity of rock material and the stiffnesses of joints. Therefore, the stiffness matrix, $[K]$ will be modified accordingly as a function of modified material parameters.

viii. The load is also modified based on the effective in-situ stresses calculated in step (vi) according to the equation,

$$\{\bar{F}_0^e\} = \int_V [B]^T \{\sigma'_0\} dV \quad (16)$$

ix. Subsequently, the deformations and induced stresses are recalculated using the effective stress concept by solving the equation,

$$[K]_{\text{modified}} \{\delta\} = \{\bar{F}_0^e + F_{\text{external}}\} \quad (17)$$

using these deformation, effective induced stresses are recalculated and added to initial effective stresses to obtain the total effective stresses.

x. The changes in the aperture follow any change in the stresses. Hence, the aperture values of the joints are updated in term of the effective stresses as,

$$e_{i+1} = f(\sigma'_{i+1}) \quad (18)$$

xi. This change in aperture brings about change in permeability of jointed rock mass and therefore is recalculated (Eq. 5).

xii. Again the seepage module is used to re-analyze based on the modified values of permeability. Total hydraulic head, Φ is found based on the new value of the aperture of joints. The pore water pressure is therefore updated according to Eqs. 13 and 14.

- xiii. The analysis may be continued till the stresses in the rock mass in two successive iterations are almost same. For that, the steps (vi – ix) are repeated.

Verified Problem

Problem Definition

The flow of water through a jointed rock mass forming the foundation of a concrete dam has been taken up for investigation. Figure 1 illustrates the configuration of the foundation and shows the geometry of the Malpasset dam in France (Bargui et al., 1998). Jointed rock media consists of rock mass intersected by two orthogonal joint sets, the first set having 20° dip while the second has a 70° dip. Both joint sets are considered as continuous due to the limitation of the continuum approach suggested in the present study. However, there are continuous and discontinuous joint sets in the field at site (Fig. 1).

In the present study, a 3D-FEM has been used for the seepage, stress and coupled stress-flow analyses. The seepage pattern and the effect of seepage on the mechanical properties of rock mass below the dam have been investigated. Hence, the study presents the variation of equipotential lines, uplift pressure below the base of the dam, and stresses and deformation pattern. This case represents a confined flow problem.

This problem was earlier attempted by Bargui et al. (1998) using a 3-D coupled mechanical-hydraulic model called BRIG3D in which attempt was made to simulate the joint sets as continuous with 70° dip and discontinuous with 20° dip.

Due to difference in configuration of the joint sets considered in the two studies, only qualitative comparison has been made.

The dam foundation consists of rock mass intersected by two orthogonal joint sets. Hydraulic and mechanical properties of the rock material and rock joints have been presented in Table 1. Stiffness values of the joints have been assumed in the present study. To accommodate the difference in continuity of the joint sets, the joint set-I (20° dip) offers stiffness ten times more than the joint set-II having 70° dip (Table 1).

Two types of loads have been considered for the stress analysis, namely the self weight of dam and the gravity load of rock foundation. For coupled stress-flow analysis, additional load comprises of hydrostatic pressure on the upstream face of the dam under full reservation condition.

In the present study the foundation domain considered for analysis is $36\text{m} \times 18\text{m} \times 16\text{m}$ in length and is illustrated by Fig. 2. By using 20-noded brick element, the domain has been discretized into 264 elements and the mesh has 1629 nodes. It has been assumed that the dam body has 6 m in width, about 12 m in height and 16 m long.

Boundary Conditions

The analysis involves two models, one for the stress analysis and the other for the seepage analysis.

- i. *Stress analysis* – A restrained condition has been imposed in vertical direction on the horizontal bottom boundary while nodes of the vertical boundary have been restrained in the lateral direction.
- ii. *Seepage analysis* – This involves two types of boundary conditions:
 - a. Dirichlet boundary condition: A head of 10 m has been applied on the upstream boundary of foundation, while zero head has been applied on the downstream side.
 - b. Neumann boundary condition: No flow has been permitted from the lower boundary and through the dam body.

Discussion of Results

1 Hydraulic characteristics

Based on various properties stated earlier, the equipotential lines have been obtained and plotted as shown in Fig. 3. In seepage analysis, where no stress has been considered, it can be seen from Fig. 3a that distribution of equipotential lines below the dam is uniform. 50% of the applied head gets dissipated near the central axis of the dam.

Coupled stress-flow analysis results in a changed pattern as depicted in Fig. 3b. The equipotential lines offset to in the downstream direction of the continuous joint set-II. Thus, it can be said that the steepest continuous joint set has a dominant effect on the hydraulic behavior under the loading. The change in pattern of the equipotential lines may be attributed to the stress effect which reduces the permeability in the region of high stress concentration.

Comparison of results obtained in the present study (Fig. 3) and those presented in Fig. 4 after Bargui et al. (1998) shows a good agreement in the trend of equipotential lines. Any inconsistency between the two studies can be attributed to the difference in assumptions and may be due to the difference in some parametric values assumed in the present study.

Figures 5a and 5b shows the pore water pressure distribution in the foundation of dam for seepage and coupled analyses respectively. An increase in the pore water pressures may be the effect of stress variation. The variation in the aperture of the joints due to loading may be accompanied by the variation in pore water pressure also.

Distribution of the uplift pressure below the base of the dam has been presented in Table 2 and plotted in Fig. 6. As expected, the higher uplift pressure has been recorded in the coupled analysis. The maximum uplift pressure below the base of dam is less than the applied stresses due to the weight of the dam.

2 Displacements

The displacement pattern in x and z-directions have been sketched in Fig. 7. It can be summarized that:

- i. Maximum deformation occurs in the region near the dam foundation.

- ii. Horizontal displacements, δ_x experiences reversal of direction in the foundation. This reversal may be attributed to the direction of slip (Fig. 7a).
- iii. The displacement contours flow along the joint planes, suggesting that the joint properties have a pronounced effect on displacements.
- iv. Saturation of rock mass in the foundation leads to an increase in the horizontal and vertical displacements, δ_x and δ_z . However, the displacement pattern remains unaltered both in stress and coupled stress-flow analysis. However, some differences in displacements have been noticed.
- v. Table 3 gives the values of the displacements below the base of the dam. Horizontal displacement, δ_x in the foundation has been found to increase due to seepage by about 10.1% below the left corner and by 6.8% below the right corner of the dam. Similarly, vertical displacement, δ_z shows an increase of about 6.7% below the left corner to about 5.0% below the right corner due to seepage.
- vi. The pattern of displacements seen in Fig. 7 has been influenced by the properties of the rock joints as well as by the type of the load applied on the surface.
- vii. The horizontal displacements in y-direction have been found to be very small.

3 Stresses

Figure 8 shows the distribution of the stresses in x, y and z-directions obtained from both stress and coupled stress-flow analyses which suggests that:

- i. Pattern of stress distribution remains unchanged in both the stress and coupled stress-flow analyses. The stress tends to flow along the joint sets.
- ii. Stresses have been found to reduce due to seepage and the pore water pressure mobilized. The effective stress reduces in the same order as pore water pressure.
- iii. Generally, the stresses are all compressive with the exception of the upper right corner of the domain considered where the horizontal stress has been found to be tensile.
- iv. The stresses increase with the depth due to consideration of the gravity component of foundation material.
- v. Table 4 gives values of stresses directly below the base of the dam. It can be seen that the horizontal stress, σ_x is more than the vertical stress, σ_z in both the analyses.
- vi. Contours of principal stresses have been displayed in Fig. 9. The pattern of stresses herein is identical for corresponding stresses.

4 Distribution of equipotential lines

To examine the effect of the modulus of elasticity of the rock material and stiffness of the joints, numerical experiments have been conducted. The material parameters employed in the numerical experiments are presented in

Table 5. Figure 10 shows the influence of modulus of elasticity of rock material and stiffnesses of the joints on the flow pattern in the foundation rock mass. In general, the changes in the mechanical properties of the rock mass constituents have altered the stresses which ultimately may be responsible for the redistribution of equipotential lines.

In case-1 where the modulus of elasticity was increased from 3000 MPa (original values) to 1700 GPa (Fig. 10a), difference in the distribution of equipotential lines has been found to be very small.

Case-2, also exhibits a small difference in equipotential lines with the increased modulus of elasticity and decreased shear stiffness (Fig. 10b). The same trend has been noticed in case-3 where the shear stiffness has increased (Fig. 10c).

To check the effect of continuity of the joints, case-4 was analyzed with the same stiffness values for the both the joint sets. Figure 10d confirmed that the pattern of equipotential lines undergoes a significant change as compared to the other cases. High stress concentration near the base of dam results into a change of the pattern of equipotential lines.

Conclusions

The coupled stress-flow analysis certainly assumes importance in the case of hydraulic structures in view of the fact that saturation of rock mass occurs in the post construction period once a reservoir is created.

Many suggestions have been found in the literature to relate the mechanical and hydraulic characteristics and various constitutive laws have been proposed. In the present study, 3D-FEM package has been developed for analyzing two independent processes of stress and flow.

The analyses presented herein, i.e. both mechanical and hydraulic analyses have displayed the capability of the software package to handle the coupled problem. The fact remains however that the joints may only be considered as continuous joints. This is one of the limitations of the continuum approach proposed in the present study.

The mechanical properties of the rock material and/or rock joints have significantly altered the results. Therefore, the choice of such appropriate properties is an important issue for accuracy of the results.

Results of the test problem show that the steepest joint set has a dominant effect on the hydraulic behavior. A good comparison has been obtained with the results obtained from other model (BRIG3D). It is finally concluded that the equivalent continuum approach has capability to capture the coupled stress-flow behavior in jointed rock mass in confined problems.

References

1. Bandis, S.C., Lumsden, A.C. and Barton N.R. (1983), "Fundamentals of Rock Joint Deformation", *Int. J. Rock Mech. Min. Sci. & Geomech. Abstr.*, Vol. 20, No. 6, pp.249-268.

2. Bargui, H., Billiotte, J. and Cojean, R. (1998), "Contribution of a 3D Model to the Analysis of the Hydromechanical Behavior of a Jointed Rock Mass Dam Foundation", *3rd Int. Conf. on Mechanics of Jointed and Faulted Rock*, Vienna (Austria), pp. 627-632.
3. Chen, M. and Bai, M. (1998), "Modeling Stress-Dependent Permeability of Anisotropic Fractured Porous Rocks", *Int. J. Rock Mech. & Min. Sci.*, Vol. 35, No. 8, pp. 1113-1119.
4. Gale, J. (1990), "Hydraulic Behaviour of Rock Joints", *Int. Symp. on Rock Joints, Loen (Norway), ISRM*, pp. 351-362.
5. Hatzor, Y. H. and Goodman, R. E. (1997), "Three-Dimensional Back-Analysis of Saturated Rock Slope in Discontinuous Rock – A Case Study", *Geotechnique*, Vol. 47, No. 4, pp. 817-839.
6. Janbu, N. (1963), "Soil Compressibility as Determined by Odometer and Triaxial Tests", *1st European Conf on Soil Mech & Found Engng*, ISSMFE, 1, Wiesbaden (Germany), pp.19-25.
7. Jing, L. and Hudson, J. A. (2004), "Fundamentals of the Hydro-Mechanical Behaviour of Rock Fractures; Roughness Characterization and Experimental Aspects", *Int. J. Rock Mech. & Min. Sci.*, Vol. 41, No. 3, Paper 1A-26.
8. Oda, M. Yamabe, T., Ishizuka, Y., Kumasaka, H., Tada, H. and Kimura, K. (1993), "Elastic Stress and Strain in Jointed Rock Masses by Means of Crack Tensor Analysis", *Rock Mech. Rock Engng.*, Vol. 26, No. 2, pp.89-112.
9. REMR (1996), "Uplift Pressures Resulting from Flow along Tapered Rock Joints", *Technical Note CS-ES-4-5*, Suppl 7, U.S. Army Engineer Waterways Experiment Station, pp. 1-11.
10. Wittke, W., Erichsen, C. and Kleinschnittger, M. (1985), "Influence of Seepage and Uplift Forces on Stresses in the Rock Foundation of Arch Dams", *5th Int. Conf. on Num. Meth. in Geomech.*, Nagoya (Japan), pp. 1787-1793.

Table 1 Material Properties (after Bargui et al., 1998)

Material Type	S. No.	Material Properties	Symbol	Unit	Value
Rock Material	1	Modulus of elasticity	E	MPa	3000
	2	Poisson's ratio	ν	-	0.20
	3	Unit weight	γ	kN/m ³	26.0
	4	Coefficient of lateral earth pressure at rest	k_o	--	0.40
Joint Set-I	5	Normal stiffness*	k_n	MPa/m	5000
	6	Shear stiffness*	k_s	MPa/m	500
	7	Aperture	e	mm	2.0
	8	Joint spacing	S_j	m	1.0
	9	Dip amount	α_j	Deg.	20
	10	Dip direction with tunnel axis	ω_j	Deg.	270
Joint Set-II	11	Normal stiffness*	k_n	MPa/m	500
	12	Shear stiffness*	k_s	MPa/m	50
	13	Aperture	e	mm	2.0
	14	Joint spacing	S_j	m	1.0
	15	Dip amount	α_j	Deg.	70
	16	Dip direction with tunnel axis	ω_j	Deg.	90

* Assumed values for the present analysis.

Table 2 Uplift Pressures below the Base of Dam

X Co-ordinates (m)	Uplift Pressure (kPa)	
	Seepage Analysis	Coupled Analysis
10.0	100.0	100.0
12.0	61.4	64.5
14.0	36.0	41.9
16.0	0.0	0.0

Table 3 Deformations along the Base of Dam

X Co-ordinates (m)	Displacement* (mm)					
	Stress Analysis			Coupled Analysis		
	δ_x	δ_y	δ_z	δ_x	δ_y	δ_z
10.0	-8.9	0.002	-19.5	-9.8	0.002	-20.8
12.0	-11.5	0.002	-20.7	-12.5	0.002	-21.7
14.0	-14.0	0.002	-21.8	-15.1	0.002	-22.8
16.0	-16.1	0.002	-22.2	-17.2	0.002	-23.3

* δ_x : horizontal displacement in x-direction, δ_y : horizontal displacement in y-direction, δ_z : vertical displacement in z-direction

Table 4 Stresses below the Base of Dam

X Co-ordinates (m)	Stresses* (MPa)					
	Stress Analysis			Coupled Analysis		
	σ_x	σ_y	σ_z	σ'_x	σ'_y	σ'_z
11.0	-0.700	-0.484	-0.401	-0.592	-0.360	-0.317
13.0	-0.676	-0.491	-0.437	-0.595	-0.394	-0.373
15.0	-0.591	-0.481	-0.581	-0.532	-0.405	-0.539

* σ_x : horizontal stress in x-direction, σ_y : horizontal stress in y-direction, σ_z : vertical stress in z-direction

Table 5 Parameters for Different Cases

Case No.	Modulus of Elasticity, E_r (MPa)	Normal Stiffness, k_n (MPa)		Shear Stiffness, k_s (MPa)	
		Joint Set-I	Joint Set-II	Joint Set-I	Joint Set-II
1	1.7×10^6	500	5000	50	500
2	1.7×10^6	500	5000	10	100
3	1.7×10^6	500	5000	100	1000
4	1.0×10^3	1000	1000	100	100

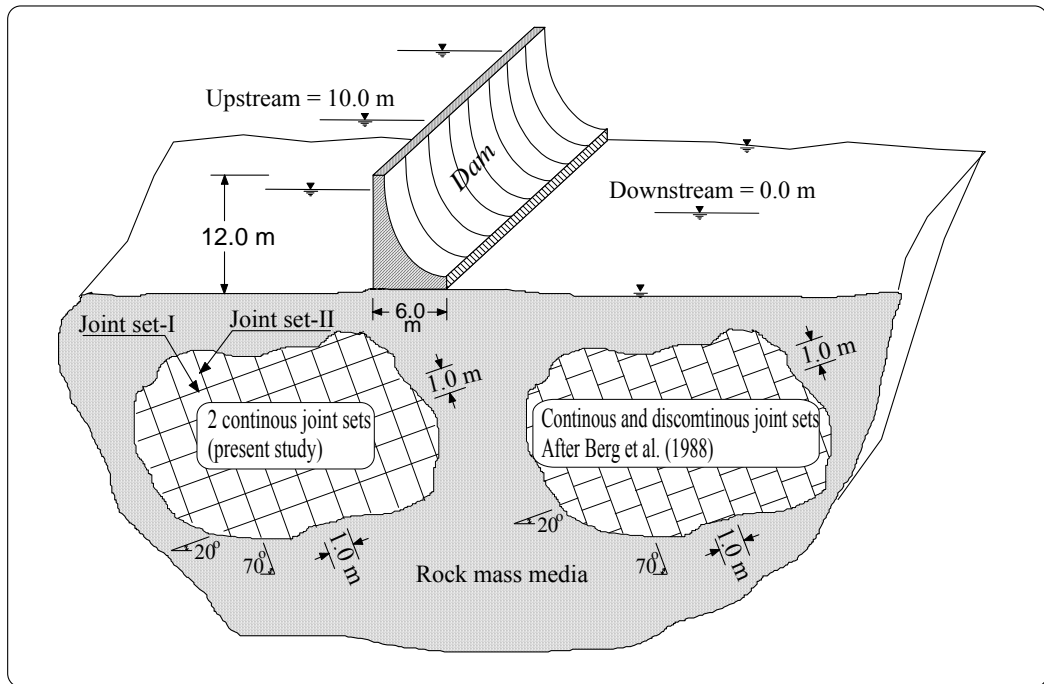


Fig. 1 Geometry of Dam Founded on Jointed Geological Formation (after Bargui et al., 1998)

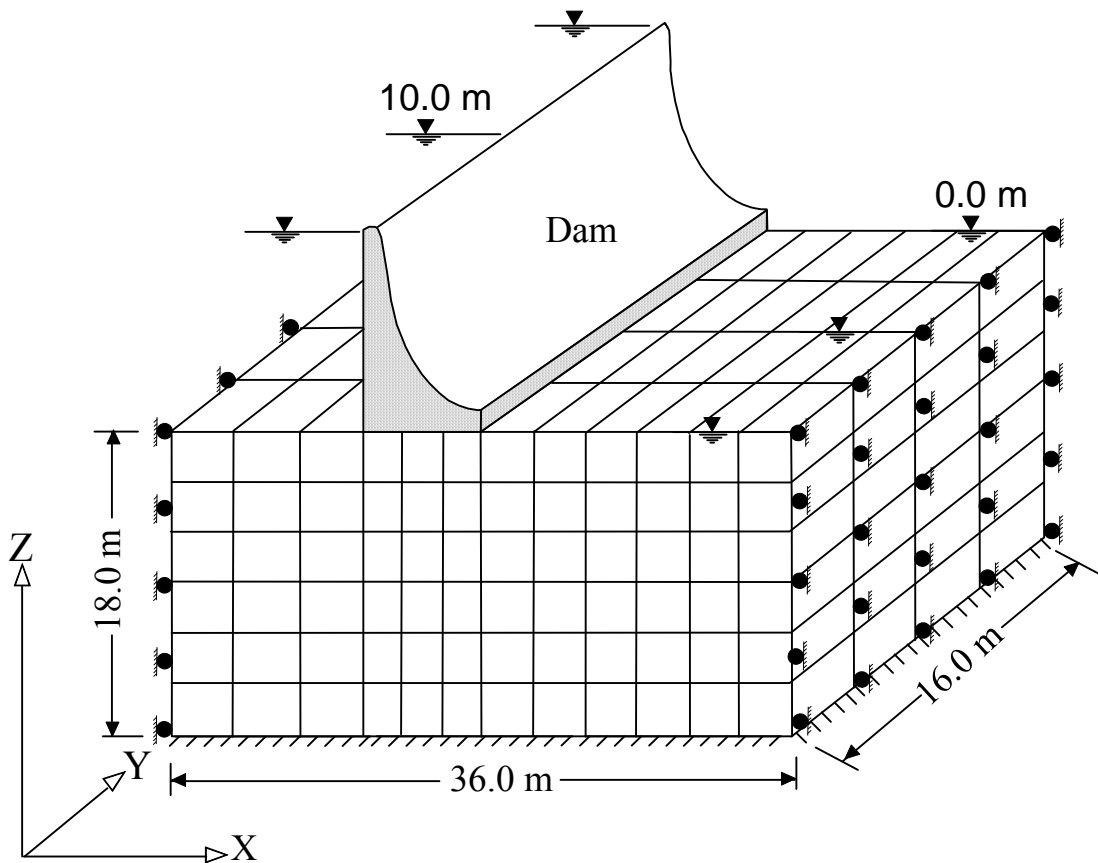
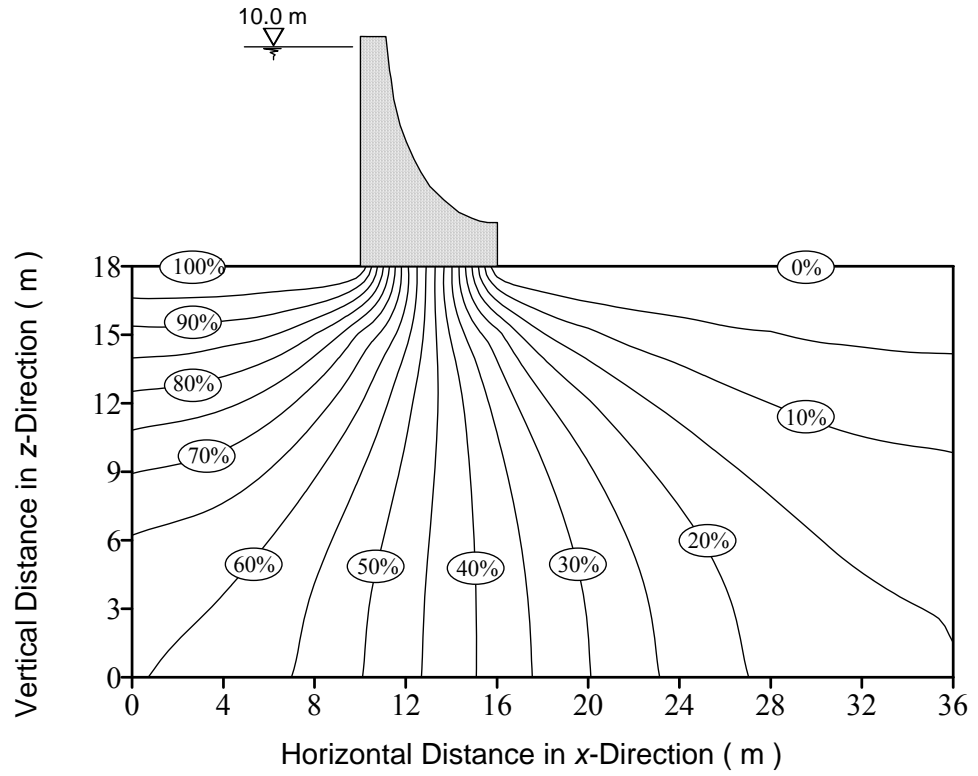
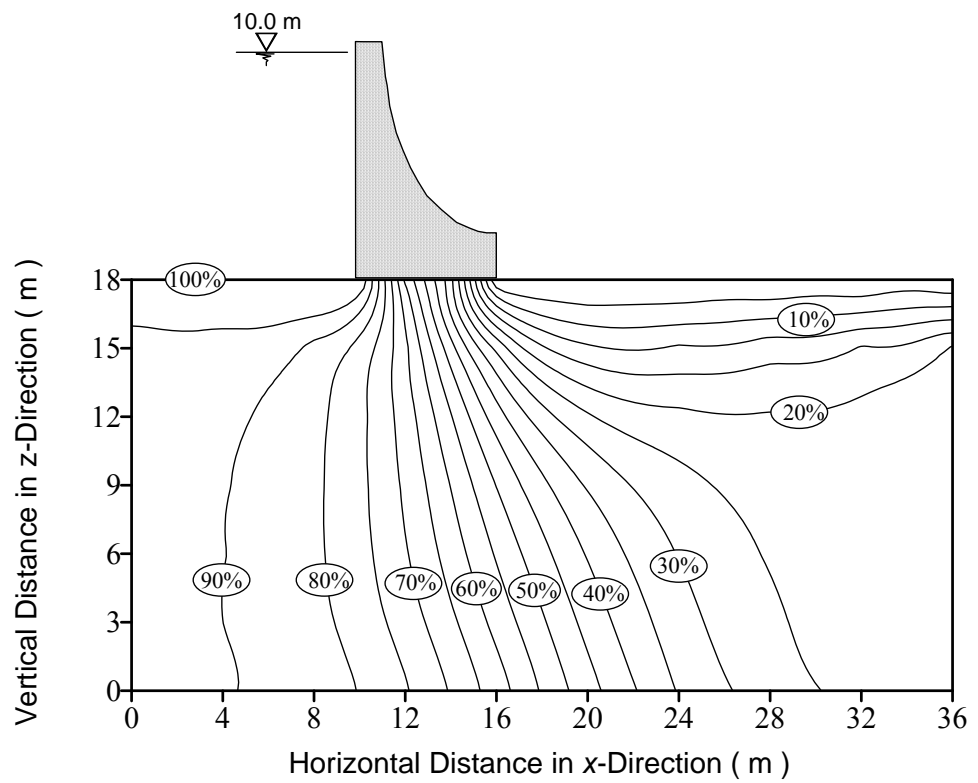


Fig. 2 3D-Finite Element Mesh of Dam-Foundation System

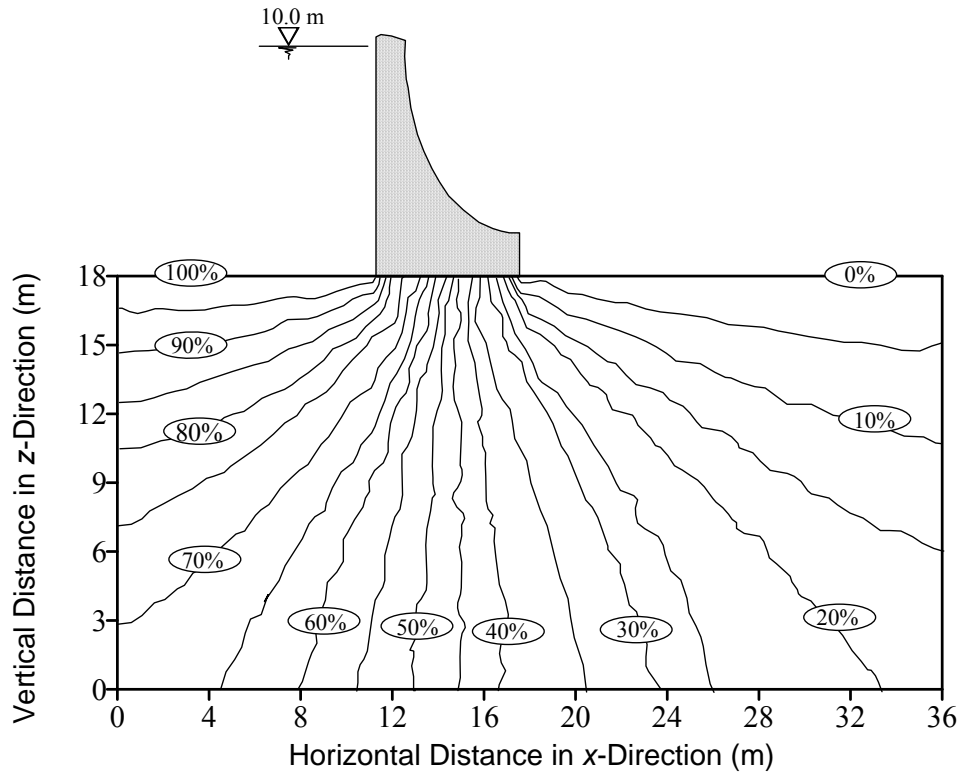


a) Seepage Analysis

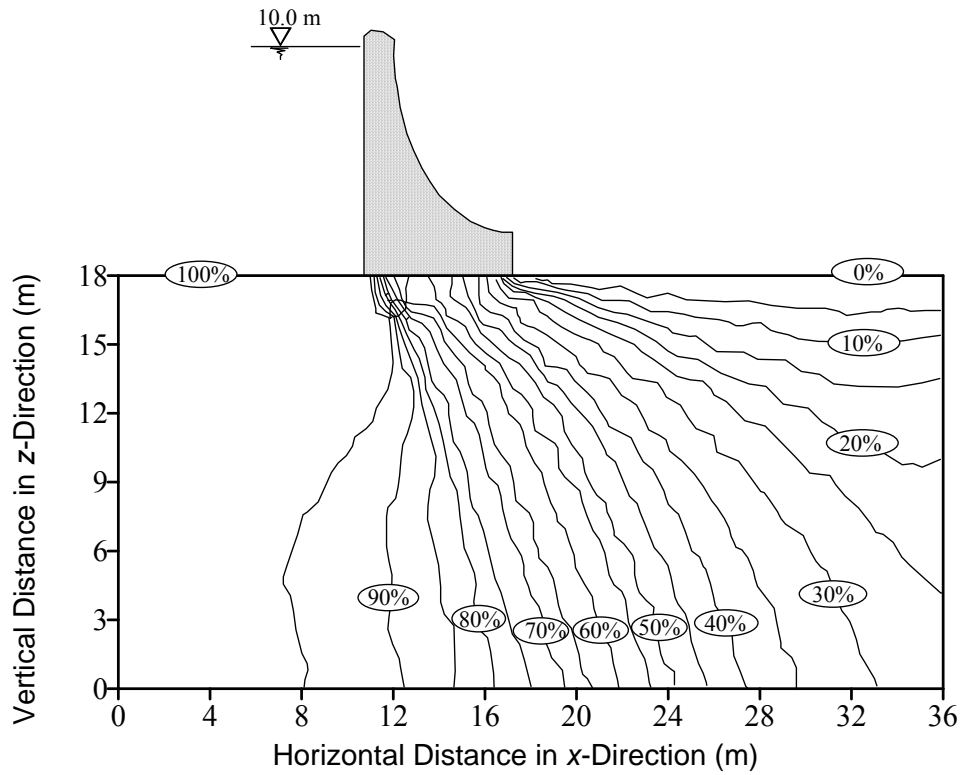


b) Coupled Analysis

Fig. 3 Contours of the Equipotential Lines below Base of Dam (Present Study)

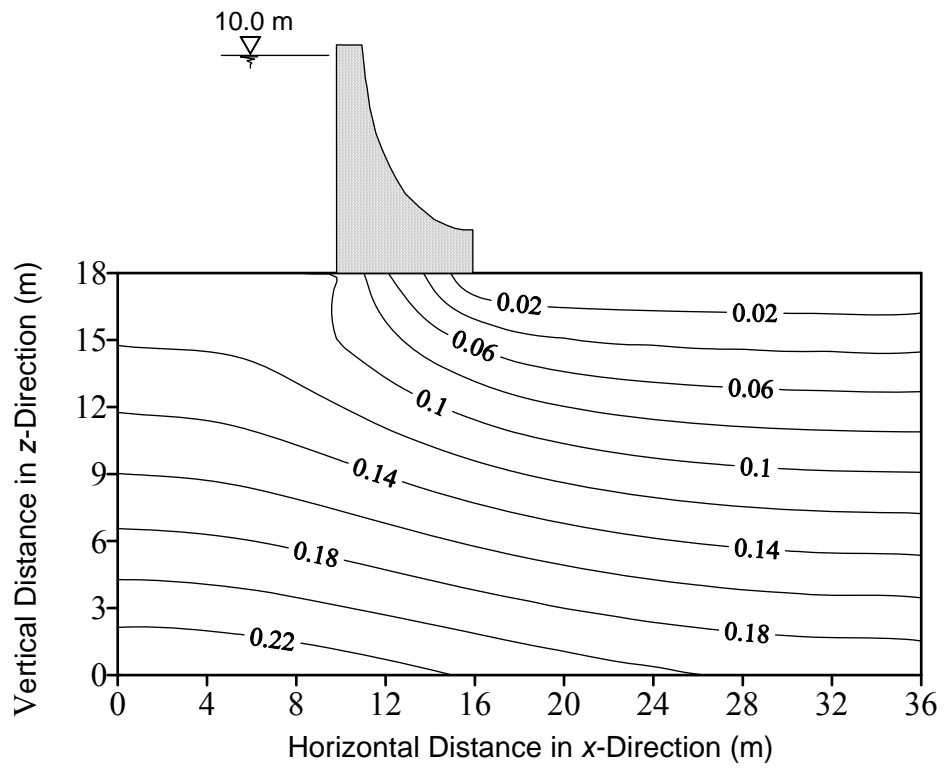


a) Seepage Analysis

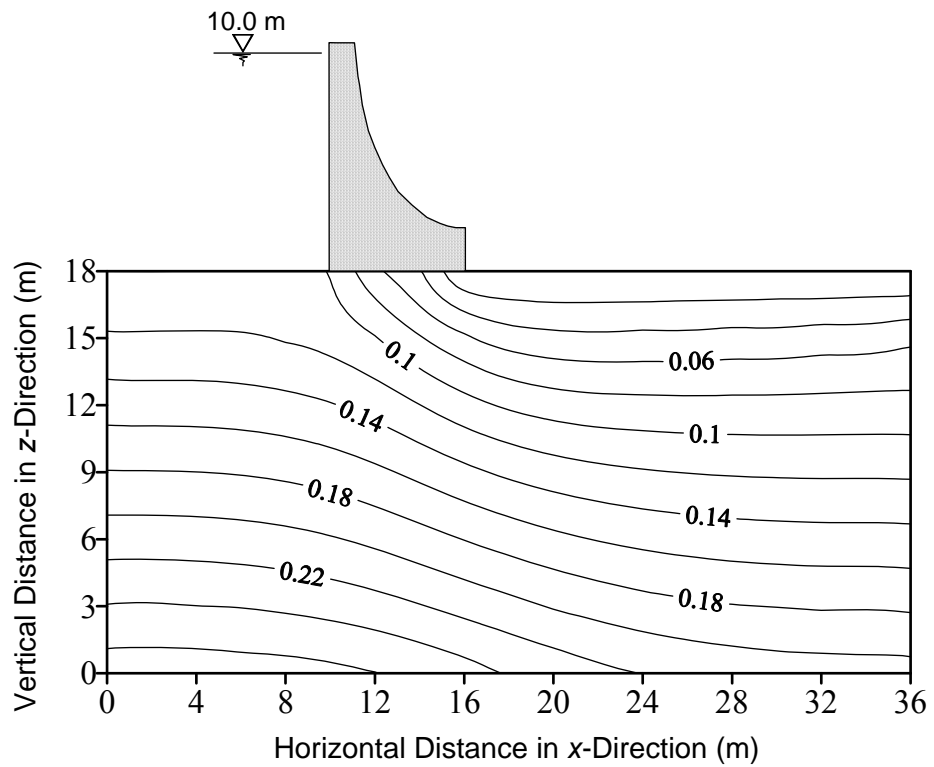


b) Coupled Analysis

Fig. 4 Distribution of Equipotential Lines in Foundation (after Bargui et al., 1998)



a) Seepage Analysis



b) Coupled Analysis

Fig. 5 Contours of Pore Water Pressure (MPa) below the Base of Dam (Present Study)

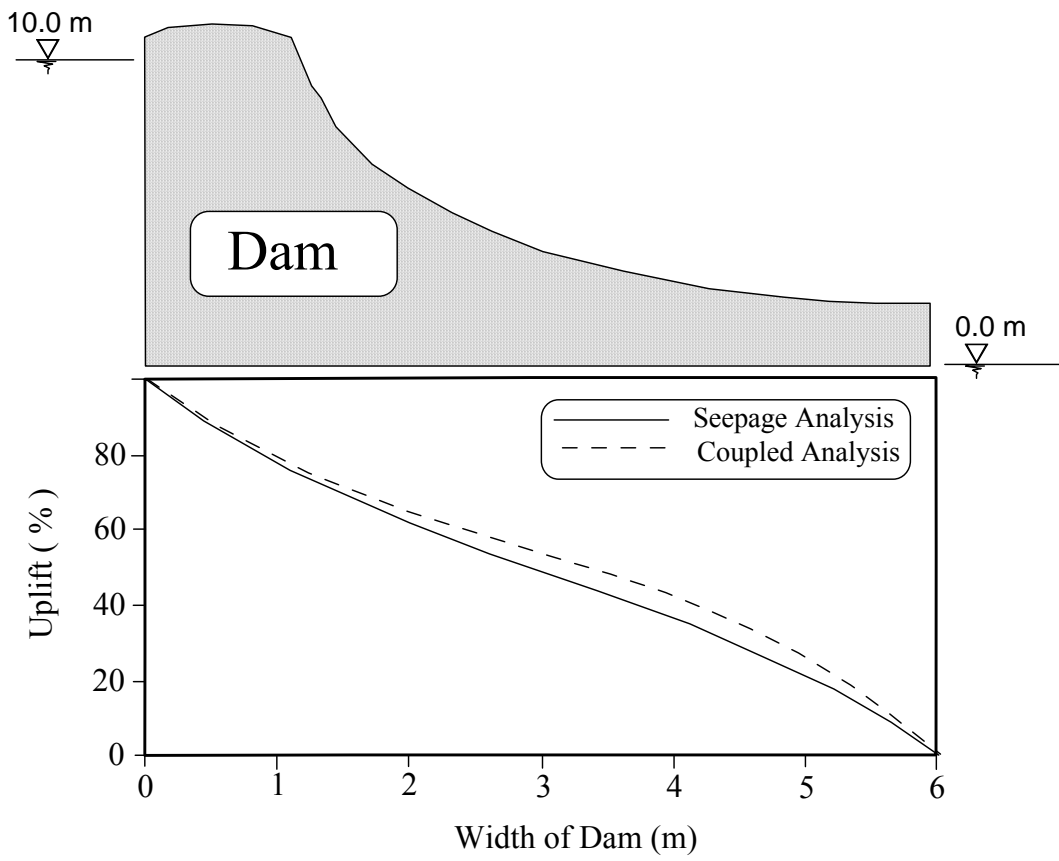
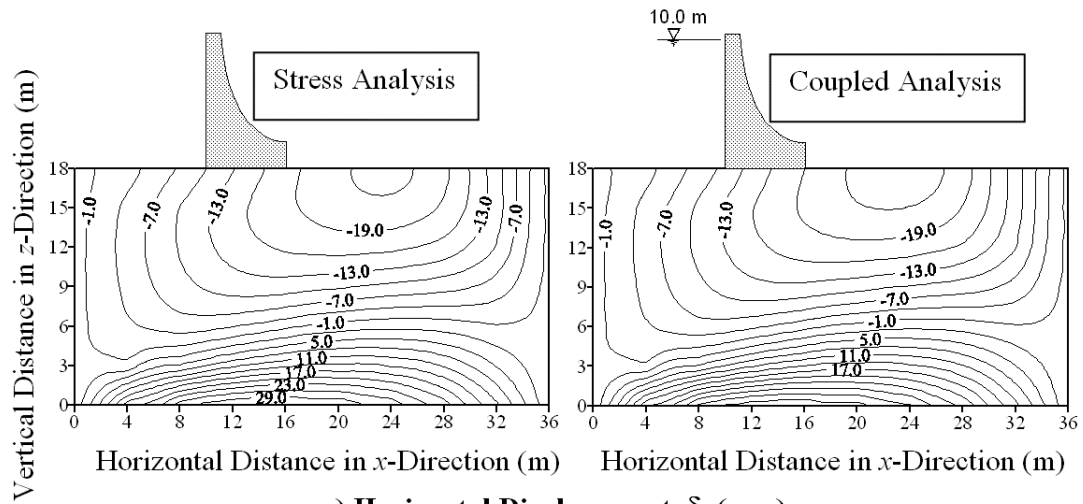
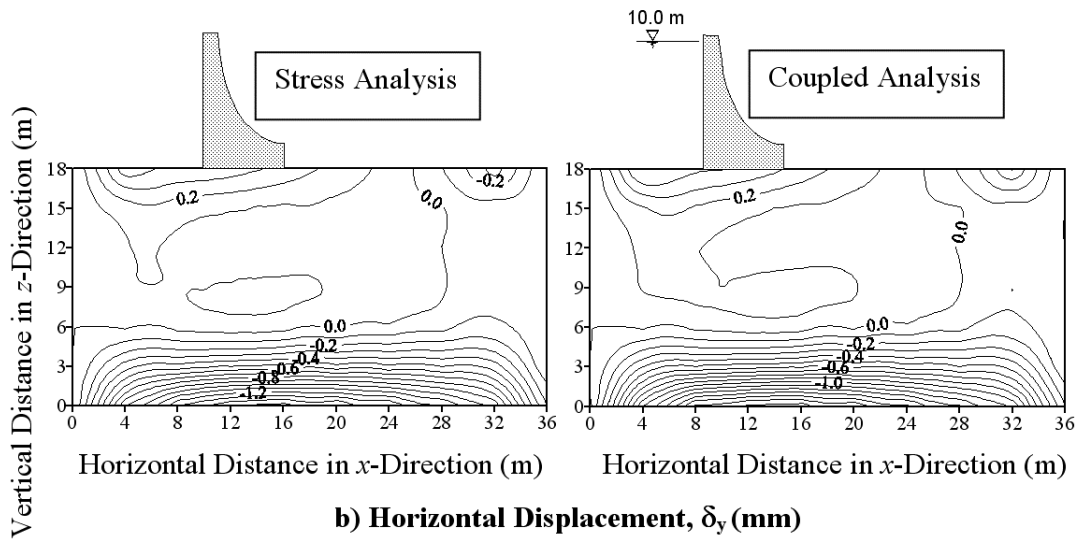


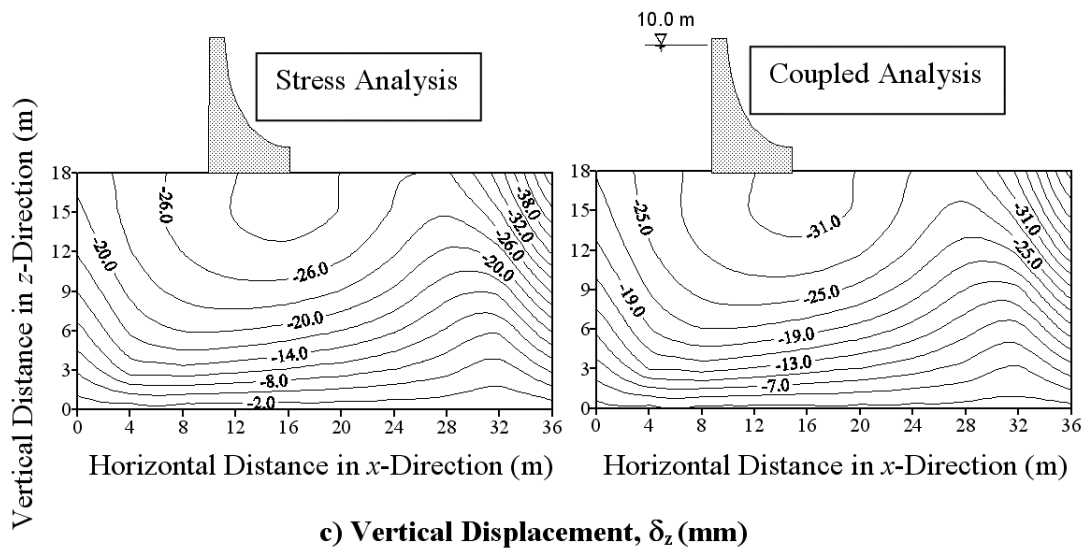
Fig. 6 Uplift Pressure (%) along the Base of Dam



a) Horizontal Displacement, δ_x (mm)

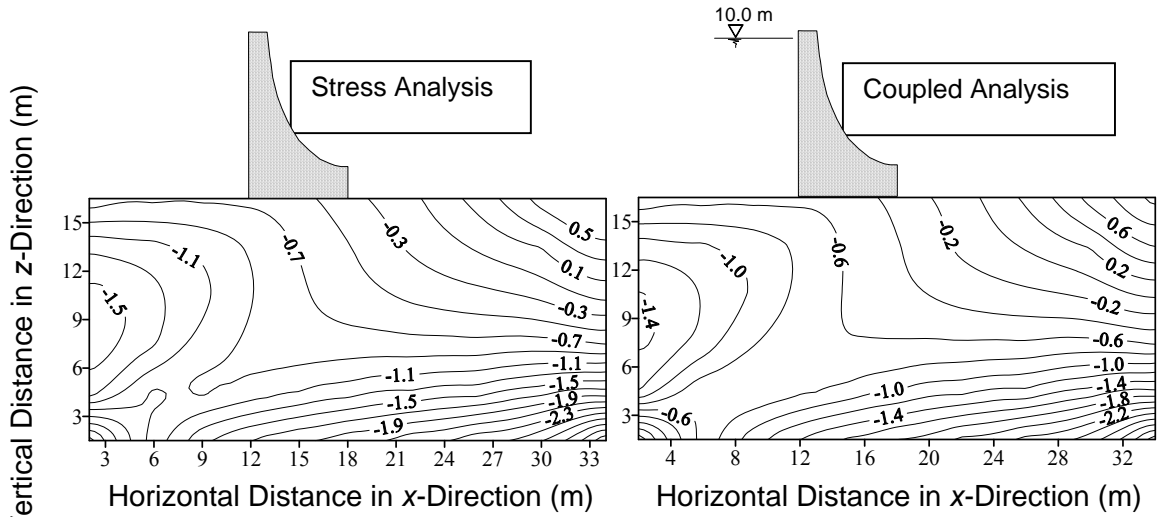


b) Horizontal Displacement, δ_y (mm)

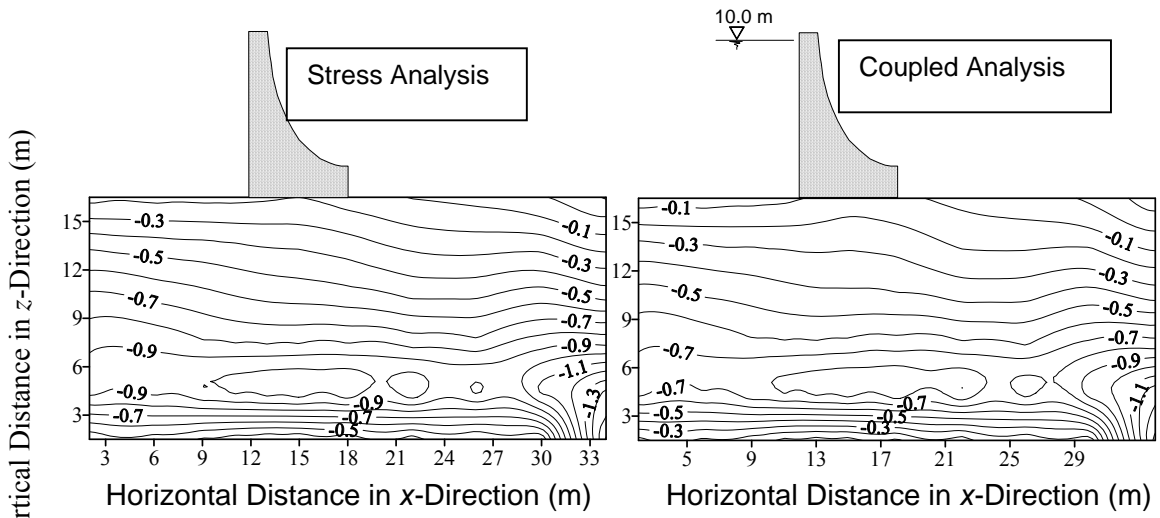


c) Vertical Displacement, δ_z (mm)

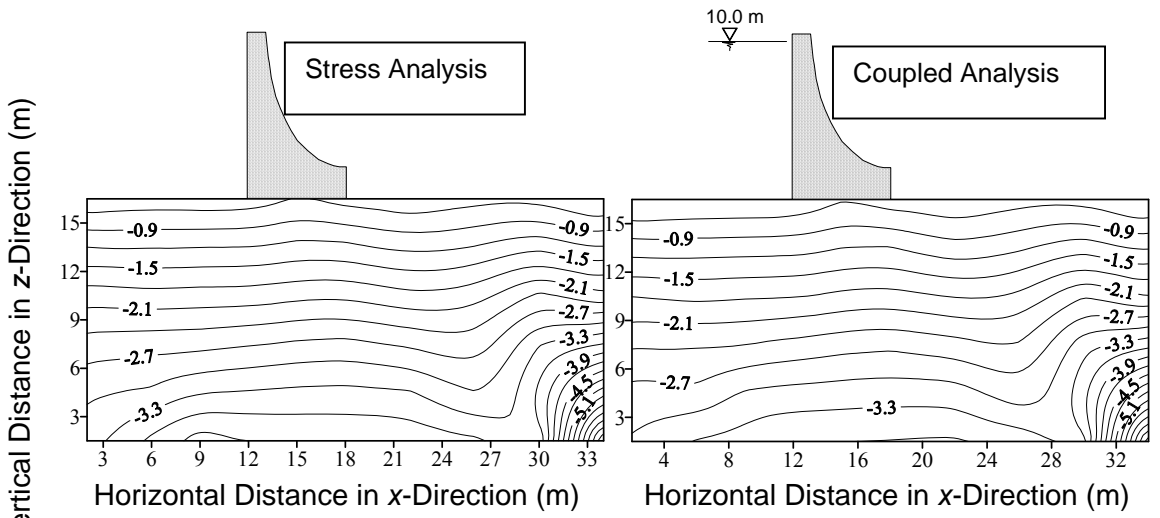
Fig. 7 Contours of Displacements below the Base of Dam



a) Horizontal Stress, σ_x (MPa)

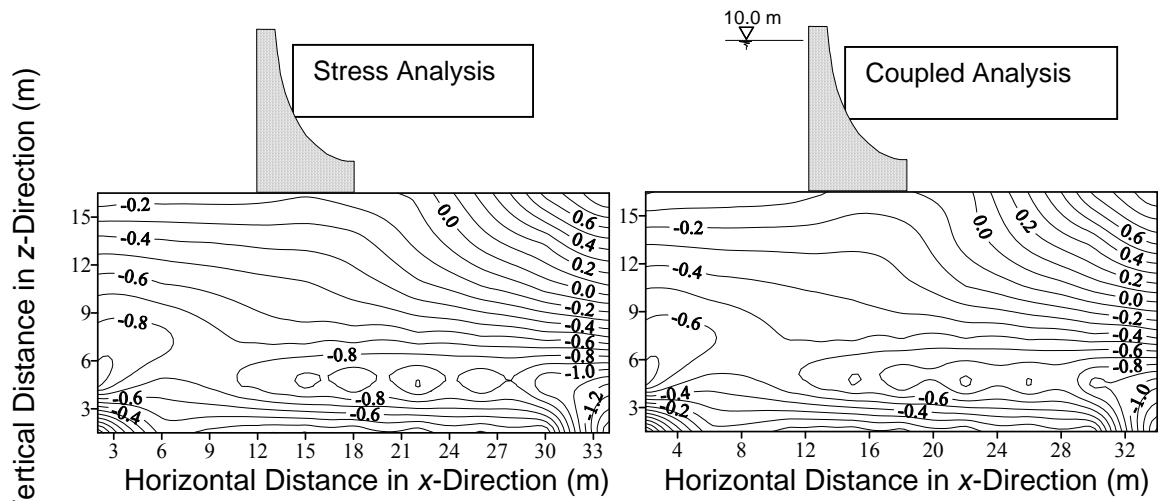


b) Horizontal Stress, σ_y (MPa)

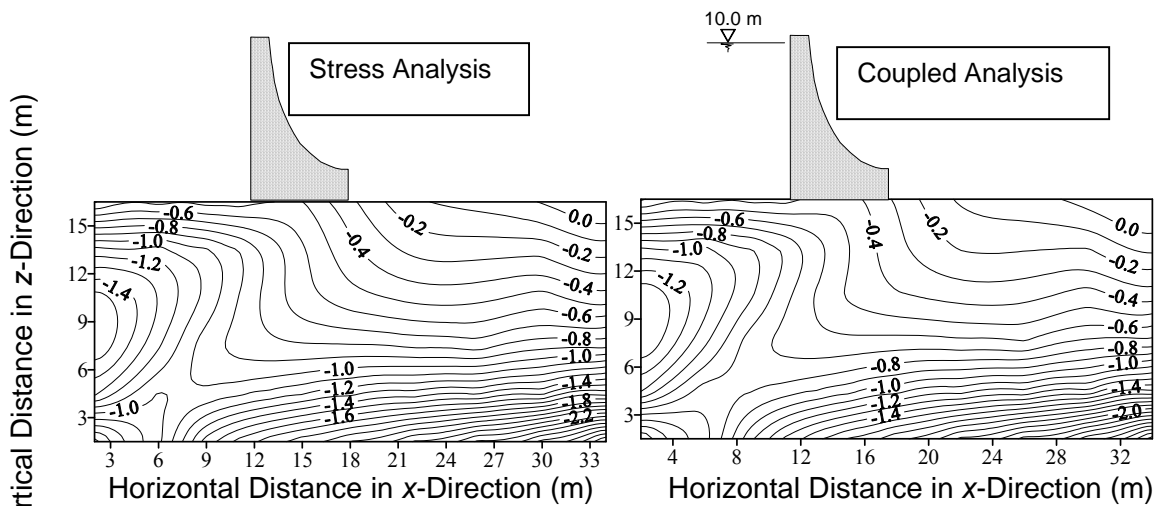


c) Vertical Stress, σ_z (MPa)

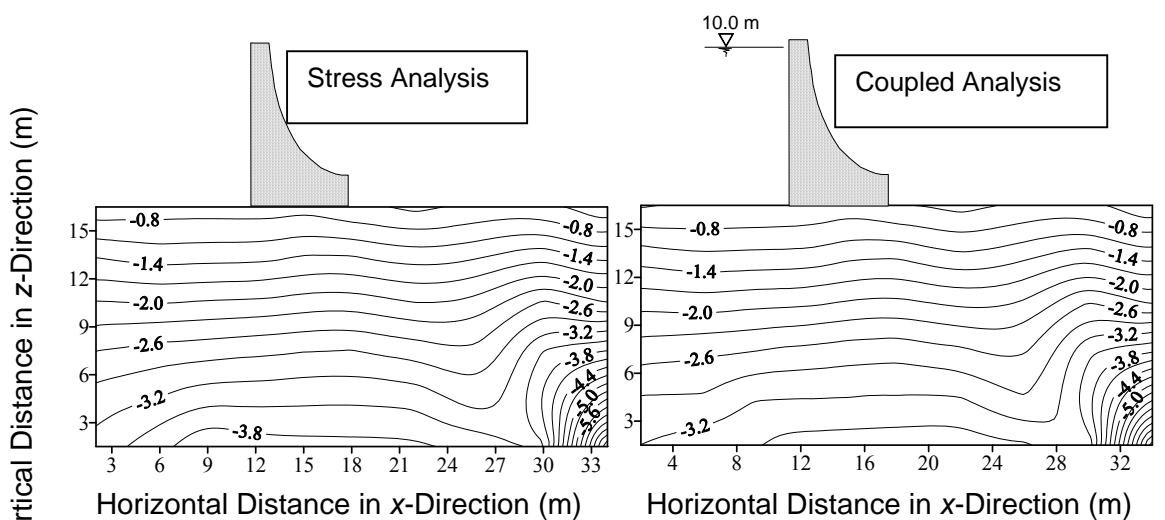
Fig. 8 Contours of Various Stresses in the Foundation of Dam



a) Minor Principal Stress, σ_3 (MPa)

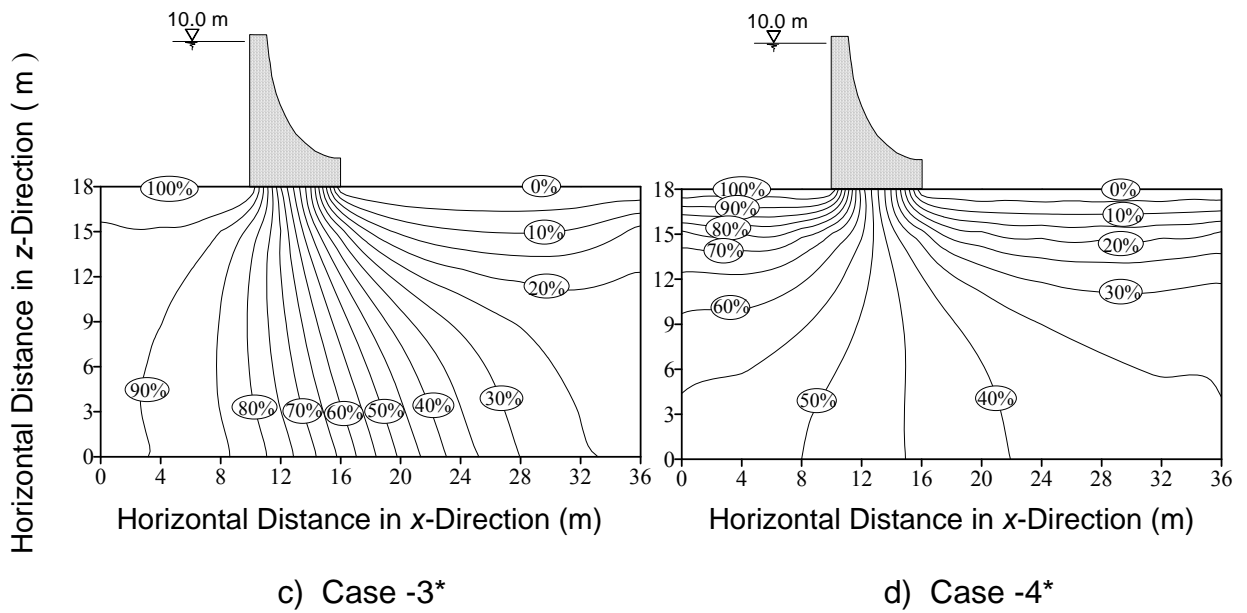
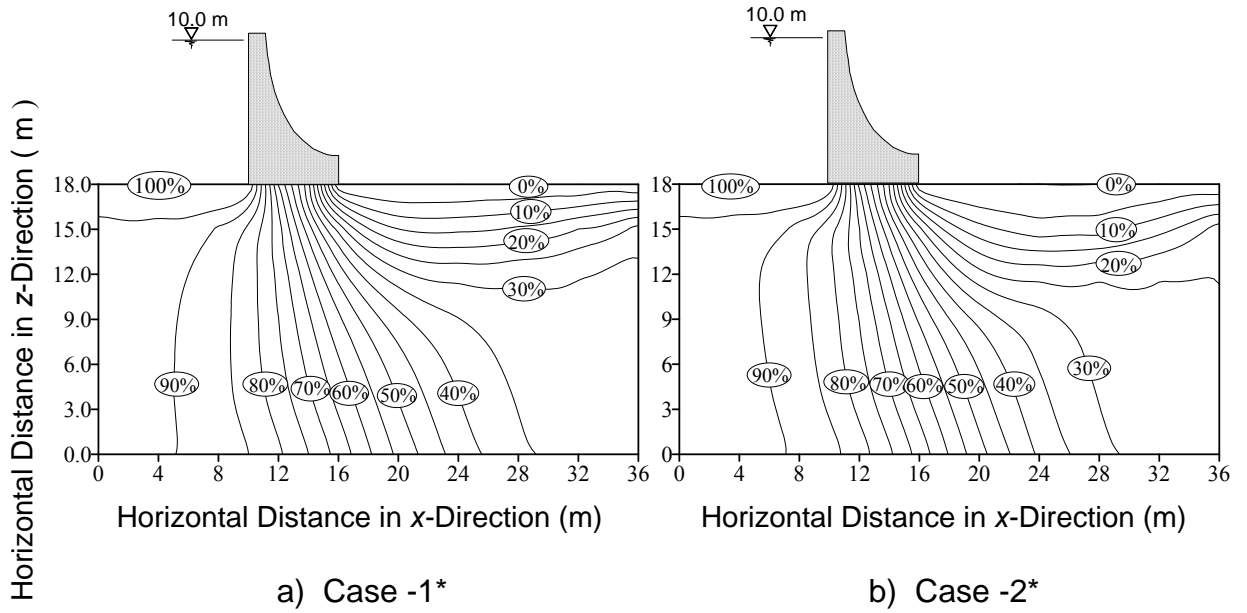


b) Intermediate Principal Stress, σ_2 (MPa)



c) Major Principal Stress, σ_1 (MPa)

Fig. 9 Contours of Principal Stresses in the Foundation of Dam



* Refer Table 5

Fig. 10 Effect of Joint Stiffnesses on Distribution of Equipotential Lines below the Base of Dam (Coupled Analysis)